

# Recent Advances in MXenes for Lithium-Ion Capacitors

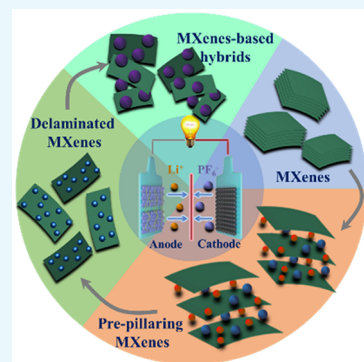
Xiong Zhang,<sup>†,‡,§,ID</sup> Lei Wang,<sup>†</sup> Wenjie Liu,<sup>†</sup> Chen Li,<sup>†,ID</sup> Kai Wang,<sup>†,‡,ID</sup> and Yanwei Ma<sup>\*,†,‡,ID</sup>

<sup>†</sup>Institute of Electrical Engineering, Chinese Academy of Sciences, No. 6 Beiertiao, Zhongguancun, Haidian District, Beijing 100190, China

<sup>‡</sup>School of Engineering Sciences, University of Chinese Academy of Sciences, Beijing 100049, China

<sup>§</sup>Dalian National Laboratory for Clean Energy, Dalian 116023, China

**ABSTRACT:** Recently, two-dimensional MXenes and MXene-based nanocomposites have become the most important electrode materials because of their unique physical and chemical characteristics. As the electrode of a lithium-ion capacitor, MXenes have exhibited metallic conductivity and plastic layer structure that provide more chemically active interfaces and shortened ion-diffusion lengths, and thus the unbalanced ion kinetics between the anode and cathode can be effectively alleviated. In order to further improve the electrochemical performance of MXenes, the composition, morphology and texture, surface chemistry, and structural configuration of MXenes are extensively investigated. In this mini-review, some recent research and progress of MXenes and MXene-based nanocomposites in lithium-ion capacitors are summarized, which focus on their nanostructure designs and chemical preparation methods, such as prepillaring MXenes, delaminated MXenes, and MXene-based hybrids. Finally, some future perspectives and critical challenges of MXene-based material for lithium-ion capacitor application are also presented and briefly discussed.



## 1. INTRODUCTION

Huge changes in the global climate and the shortage of fossil fuels require the society to acquire green and sustainable energy. Among various renewable storage devices, electrochemical energy storage (EES) devices stand out based on their high-energy efficiency and high performance.<sup>1</sup> Thus, they have been extensively applied in portable electronic devices, smart grids, and hybrid electric vehicles (HEVs). The energy density for state-of-the-art lithium-ion battery (LIB) is about 200 Wh kg<sup>-1</sup>. However, the intrinsic sluggish diffusion process of Li<sup>+</sup> into the bulk material impedes the power performance of LIBs (usually <2 kW kg<sup>-1</sup>), which causes an inferior acceleration rate in HEVs.<sup>2</sup> On the contrary, supercapacitors (SCs), which are known for their high power density (>10 kW kg<sup>-1</sup>) and excellent cycling life (>10<sup>5</sup> cycles), suffer from unsatisfactory energy density (about 5–10 Wh/kg) since charge storage is mainly on/near the surface of porous materials.<sup>3</sup> Hence, it is urgent to find an effective way to achieve a trade-off between LIBs and SCs.

In recent years, a new energy storage device lithium-ion capacitor (LIC), which is assembled by a LIB-type anode and a SC-type cathode with an appropriate electrolyte (contains lithium salt), has been a hot topic in the complementation of LIBs and SCs.<sup>4</sup> The charge capture mechanism for the LIC is illustrated in Figure 1a.<sup>5</sup> The energy storage and release for the conventional LIB-type materials are primarily derived from the insertion/deinsertion of the lithium ion, which are determined by the Li<sup>+</sup> diffusion rate into the bulk of material. Besides, PF<sub>6</sub><sup>-</sup> from the electrolyte is rapidly absorbed/desorbed on/near the surface of SC-type electrodes, and thus a considerable power density can be achieved.<sup>6</sup> Up to now, various constructions of

LICs have been reported with gratifying results. However, the obstacle for practical application of LICs is still huge due to the limited capacity of SC-type material and the imbalance of charge storage kinetic between the two kinds of electrodes. These inevitably lead to the capacity mismatch between the anode and cathode, resulting in a low energy density of the LIC. Therefore, the critical issue in developing high-performance LICs is to utilize suitable anode and cathode materials with matched kinetics.

So far, a variety of electrode materials have been exploited in the LIC devices. On account of the different Li-ion storage mechanisms, the anode materials for LICs can be divided into three categories.<sup>10</sup> First, insertion-type materials, such as graphite, hard carbon, TiO<sub>2</sub>, Li<sub>4</sub>Ti<sub>5</sub>O<sub>12</sub> (LTO), and Nb<sub>2</sub>O<sub>5</sub>, have the advantage of stable structure. However, the inferior capacity (<400 mAh g<sup>-1</sup>) or high-voltage platform versus Li metal impedes the full energy utilization. Then the alloy-type (Si, Sn, and Sn-based composites) and conversion-type (Fe<sub>3</sub>O<sub>4</sub>, CoO, MoS<sub>2</sub>, and MnO<sub>2</sub>) materials can deliver high theory capacity (>700 mAh g<sup>-1</sup>). Nevertheless, the high irreversible capacity, huge volume variation, and poor kinetics of these materials cause severe electrode polarization and capacity decay during the long-term cycling. Hence, for LIC anode materials, the key issues are fixating on improving the electronic/ion conductivity and cycle stability. From this aspect, materials with well-designed or nanosized structure can effectively shorten the Li<sup>+</sup> diffusion path and improve the

Received: October 30, 2019

Accepted: December 4, 2019

Published: December 18, 2019

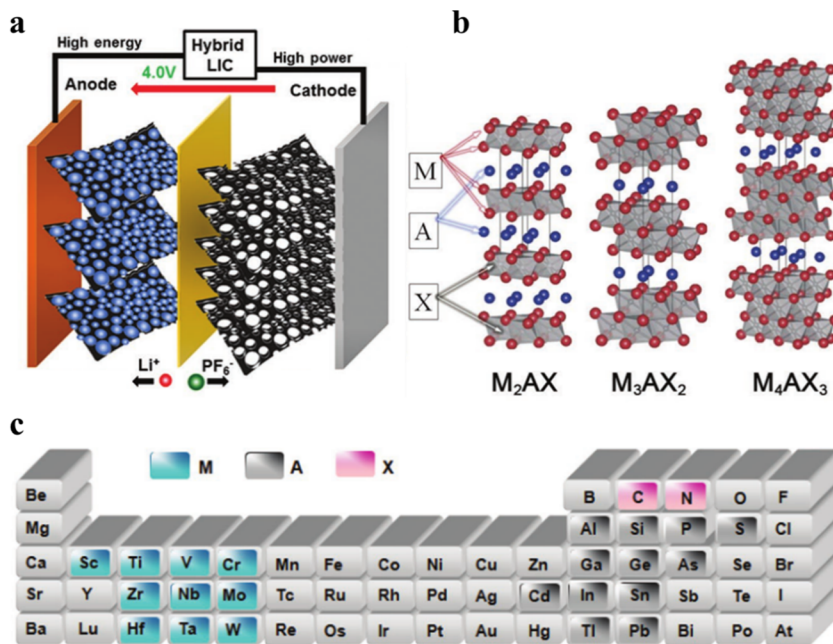


**Figure 1.** (a) Energy-harvesting mechanism of LIC in the charging process.<sup>7</sup> (b) Atomic structures of  $M_2AX$ ,  $M_3AX_2$ , and  $M_4AX_3$  phases.<sup>8</sup> (c) The fragment of the element that makes up the MAX phase of the general composition  $M_{n+1}AX_n$  in the periodic table. Fragment of the periodic table<sup>9</sup> (reprinted with permission from refs 7–9).

electron transport.<sup>11</sup> At present, carbonaceous materials such as activated carbon (AC), graphene, and carbon nanotubes (CNTs) are the frequently used materials in LIC cathodes. Among various SC-type materials, AC has received wide attention due to its high specific surface area, simple preparation, and low cost. However, its large narrow and tortuous pore channels prevent the diffusion of the electrolyte ion, and the relatively low electron conductivity causes an inferior capacity. Thus, cathode materials with large surface area and suitable pore-size distribution can effectively improve the capacity and power performance of LICs.

Recently, two-dimensional (2D) materials have triggered a new round of research hotspots since their unique structure affords more access in contact with the electrolyte and improves the ion transport rate. Graphene, as the first successfully prepared 2D material, has the advantages of remarkably electric conductivity, high surface area ( $\sim 2630\text{ m}^2/\text{g}$  in theory), and excellent thermal stability.<sup>12</sup> However, the low tap density and suffering from restacking of 2D graphene prevent it from suitable electrode materials for the LIC applications.<sup>13</sup> MXenes, which are known as the rising star in the family of 2D materials, consist of transition metal carbides, nitrides, and carbonitrides (generally denoted as  $M_{n+1}X_nT_x$ , where M stands for an early transition metal Ti (Nb et al.), X is the C or N element, and  $T_x$  indicates different surface termination polar groups such as  $-\text{OH}$ ,  $-\text{O}$ , and  $-\text{F}$ ).<sup>14</sup> MXenes are always prepared by selectively extracting the A element layers (A is generally the main group IIIA or IVA) from the corresponding three-dimensional  $M_{n+1}AX_n$  ( $n = 1–3$ ) phases (Figure 1b,c). MXenes have been extensively investigated in various applications, especially as a high-performance electrode in LIBs and SCs, which are ascribed to their metallic conductivity (up to  $10^5\text{ S/m}$ ),<sup>15</sup> high density ( $\sim 3.8\text{ g/cm}^3$ ),<sup>16</sup> mechanical stability, and excellent hydrophilicity.<sup>17</sup> Moreover, the abundant active sites and negatively charged surfaces of 2D MXenes result in the great capability of

charge storage and release.<sup>18</sup> Stimulated by these exciting properties, MXenes are becoming promising candidate materials for the next-generation LIC application, and plenty of infusive achievements based on MXenes have emerged. Hence, it is necessary to update the latest developments of MXenes or MXene-based materials.

In this mini-review, we are committed to summarizing the recent research progress of MXenes and their derivatives in advanced LIC devices. At first, a short introduction for the electrode materials of LICs is provided. Subsequently, we propose to give a comprehensive and vital summary of the latest advanced MXene or MXene-based materials, which are used as the electrodes for high-performance LICs. Finally, there are some critical challenges and outlooks of 2D MXene materials generalized to highlight the future direction of LICs.

## 2. APPLICATIONS TO LITHIUM-ION CAPACITORS

As a hybrid electrochemical full cell, the LIC needs a large-capacity anode with reversible Li<sup>+</sup> intercalation to achieve advanced electrochemical energy storage. MXenes, including  $\text{Ti}_3\text{C}_2\text{T}_x$ ,  $\text{Ti}_2\text{CT}_x$ ,  $\text{Nb}_2\text{CT}_x$ , and  $\text{V}_2\text{CT}_x$ , possess novel ultrathin and open-layer structure, which relieve the sluggish intercalation/deintercalation kinetics of Li ions. So, MXenes present nonideal battery behavior but are similar to a capacitor, which indicates their application in lithium-ion capacitors.<sup>19,20</sup> Furthermore, the energy storage property, electronic transmission speed, and stability of MXenes are affected significantly by functional groups ( $-\text{F}$ ,  $-\text{OH}$ ,  $-\text{O}$ ,  $-\text{Cl}$ ) on the surface of MXene layers.

**2.1.  $\text{Ti}_3\text{C}_2\text{T}_x$  MXenes.**  $\text{Ti}_3\text{C}_2\text{T}_x$ , the typical representative among MXenes, is extensively studied according to its metallic conductivity and great chemical stability in fluoride-based acidic solutions.<sup>21</sup>  $\text{Ti}_3\text{C}_2\text{T}_x$  is prepared through selectively etching Al layers from the  $\text{Ti}_3\text{AlC}_2$  (MAX) in HF and LiF/HCl. Therefore, various termination groups ( $-\text{OH}$ ,  $-\text{F}$ ,  $-\text{O}$ ,  $-\text{Cl}$ ), which affect its physical and chemical properties, are

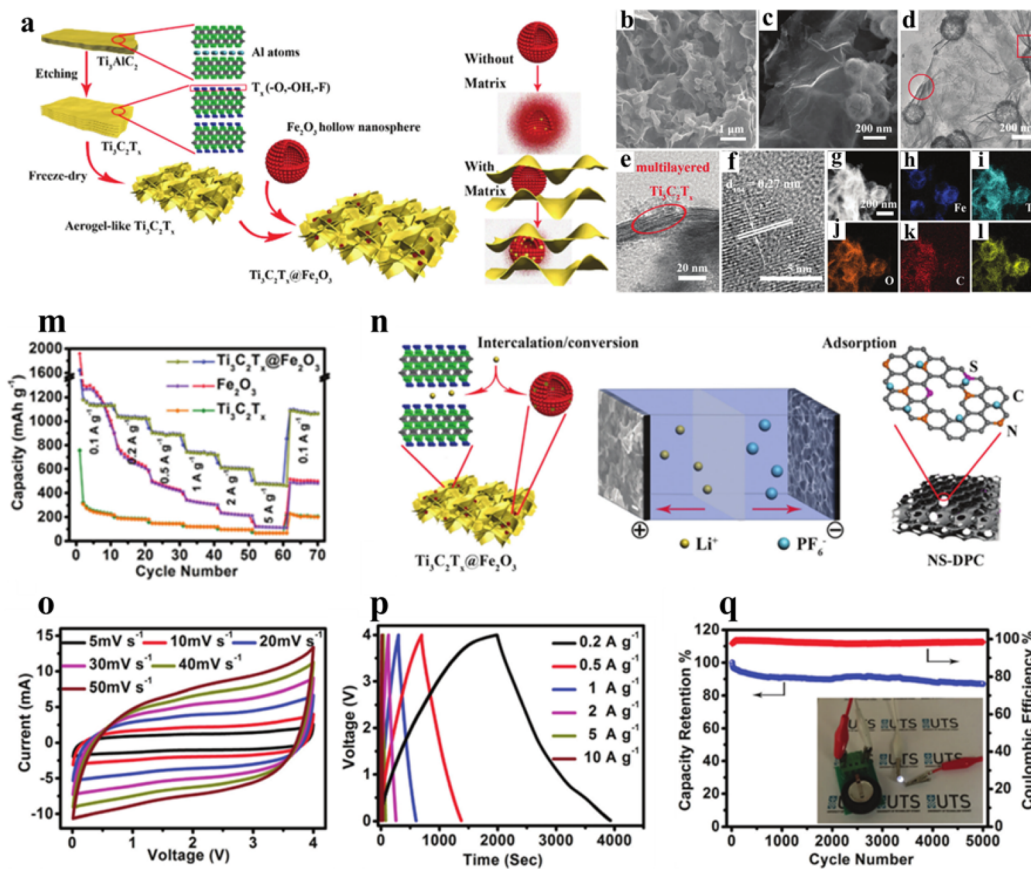


**Figure 2.** (a) Schematic illustration of the synthesis procedure for the  $\text{Ti}_3\text{C}_2\text{T}_x@\text{Fe}_2\text{O}_3$  nanocomposite. (b) SEM images of the  $\text{Ti}_3\text{C}_2\text{T}_x@\text{Fe}_2\text{O}_3$  nanocomposite. (c–f) TEM and HRTEM image of the  $\text{Ti}_3\text{C}_2\text{T}_x@\text{Fe}_2\text{O}_3$  nanocomposite. (g–l) Elemental mapping of the  $\text{Ti}_3\text{C}_2\text{T}_x@\text{Fe}_2\text{O}_3$  nanocomposite. (m) Rate performances of  $\text{Fe}_2\text{O}_3$ ,  $\text{Ti}_3\text{C}_2\text{T}_x$ , and  $\text{Ti}_3\text{C}_2\text{T}_x@\text{Fe}_2\text{O}_3$  electrodes. (n) Schematic illustration of the charge-storage mechanisms for the  $\text{Ti}_3\text{C}_2\text{T}_x@\text{Fe}_2\text{O}_3//\text{NS-DPC}$  LIC device. (o,p) CV and charge–discharge curves of the LIC. (q) Cycling stability of the LIC at a current density of  $5 \text{ A g}^{-1}$  (reprinted with permission from ref 23).

carried out on the  $\text{Ti}_3\text{C}_2\text{T}_x$  surface.<sup>22</sup> In addition, these functional groups are in between  $\text{Ti}_3\text{C}_2\text{T}_x$  layers and function as “pillars”, leading to an original interlayer spacing of 0.977 nm for the unmodified  $\text{Ti}_3\text{C}_2\text{T}_x$ .<sup>5</sup> Moreover, the stable interlayer space facilitates the contact between the  $\text{Ti}_3\text{C}_2\text{T}_x$  surface and electrolyte ions. Yet, according to previous reports, the existence of “pillars” on the surface of  $\text{Ti}_3\text{C}_2\text{T}_x$  may reduce the storage capacity for  $\text{Li}^+$ .<sup>17</sup> When the  $\text{Ti}_3\text{C}_2\text{T}_x$  is used as an anode for the lithium half-cell, only 70–225 mAh g<sup>-1</sup> (gravimetric capacity) can be realized, and even the theoretical capacity of  $\text{Ti}_3\text{C}_2\text{T}_x$  is predicted to be 320 mAh g<sup>-1</sup>.<sup>4</sup> So, if the interlayer space of  $\text{Ti}_3\text{C}_2\text{T}_x$  is rationally increased and utilized, the ability of fast Li-ion (de)intercalation will be further improved. Meanwhile, the unbalanced ion kinetics between the faradaic battery-type anode and the nonfaradaic capacitive cathode in LICs will be reduced.

One effective solution is to use electrochemical active materials acting as pillars, which can effectively exploit the potential storage space and resolve the low capacity issue for unmodified  $\text{Ti}_3\text{C}_2\text{T}_x$ . Tang et al. prepared  $\text{Ti}_3\text{C}_2\text{T}_x@\text{Fe}_2\text{O}_3$  nanocomposites via a kind of surfactant and then used them as an anode for LICs (Figure 2a).<sup>23</sup>  $\text{Fe}_2\text{O}_3$  hollow nanospheres are uniformly and perpendicularly located on the  $\text{Ti}_3\text{C}_2\text{T}_x$  surface (Figure 2b–d). The interlayer space of multilayered  $\text{Ti}_3\text{C}_2\text{T}_x$  (0.977 nm) (Figure 2e) is much larger than the diameter of  $\text{Li}^+$  (0.76 Å). As shown in Figure 2g–l, elemental mapping proves that  $\text{Fe}_2\text{O}_3$  in between the interlayer of

$\text{Ti}_3\text{C}_2\text{T}_x$  is evenly distributed. Furthermore, the nanocomposites can achieve a fast Li-ion (de)intercalation kinetics and an impressive specific capacity of 1180 mAh g<sup>-1</sup> at a current density of 0.1  $\text{A g}^{-1}$  (Figure 2m). Afterward, an LIC is assembled based on the  $\text{Ti}_3\text{C}_2\text{T}_x@\text{Fe}_2\text{O}_3$  anode and the three-dimensional nitrogen and sulfur dual-doped porous carbon (NS-DPC) as the cathode (Figure 2n). In this system, the capacitor-type cathode has rich mesoporous structure, and the ion diffusion distance between the proton and electrolyte is short; therefore, the rate capability of the LIC device can be enhanced. The  $\text{Ti}_3\text{C}_2\text{T}_x@\text{Fe}_2\text{O}_3//\text{NS-DPC}$  LIC can achieve a high energy density (216 Wh kg<sup>-1</sup>) with a power density of 400 W kg<sup>-1</sup>. Moreover, the CV curves (Figure 2o) present a quasi-rectangular shape, which implies a better capacitive behavior and fast charge/discharge rate of LICs. The GCD curves shown in Figure 2p have near-linear slope and a specific capacity of 109 mAh g<sup>-1</sup> (at 0.2  $\text{A g}^{-1}$ ), which based on the total mass of the active substance for both the cathode and anode can be achieved. In addition, the LIC delivers a prolonged cycle life with 87% of the initial capacity retention after 5000 cycles at 5  $\text{A g}^{-1}$  (Figure 2q).

Similar to the work of  $\text{Ti}_3\text{C}_2\text{T}_x@\text{Fe}_2\text{O}_3//\text{NS-DPC}$  LIC, Luo et al. prepared a pillared MXene (CTAB-Sn(IV)@ $\text{Ti}_3\text{C}_2$ ) anode by a facile liquid-phase cetyltrimethylammonium bromide (CTAB) prepillaring and  $\text{Sn}^{4+}$  pillaring method (Figure 3a).<sup>5</sup> The interlayer distance of  $\text{Ti}_3\text{C}_2\text{T}_x$  reaches 2.230 nm in comparison with the original size of 0.977 nm.

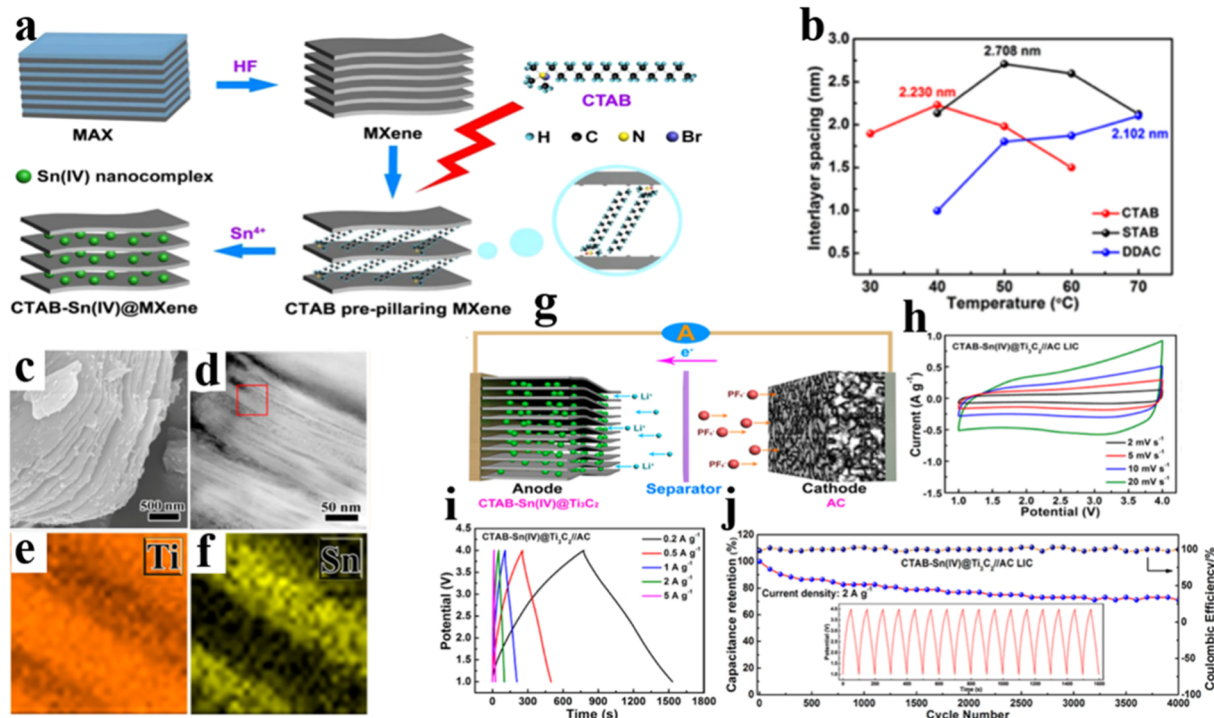


**Figure 3.** (a) Schematic illustration of the preparation of CTAB-Sn(IV)@Ti<sub>3</sub>C<sub>2</sub> by HF etching, CTAB prepillaring, and Sn<sup>4+</sup> pillaring methods. (b) Interlayer spacing of cationic surfactants (CTAB, STAB, DDAC) of prepillared Ti<sub>3</sub>C<sub>2</sub> at different treatment temperatures (30–70 °C). (c–f) SEM, STEM image of CTAB@Ti<sub>3</sub>C<sub>2</sub>, and corresponding elemental mapping of Ti and Sn. (g) Charging process of CTAB-Sn(IV)@Ti<sub>3</sub>C<sub>2</sub>//AC LIC. (h) CV curves of LIC at different scan rates. (i) GCD curves of LIC at different current densities. (j) The cycling stability of the LIC at the current of 2 A g<sup>-1</sup> (reprinted with permission from ref 5).

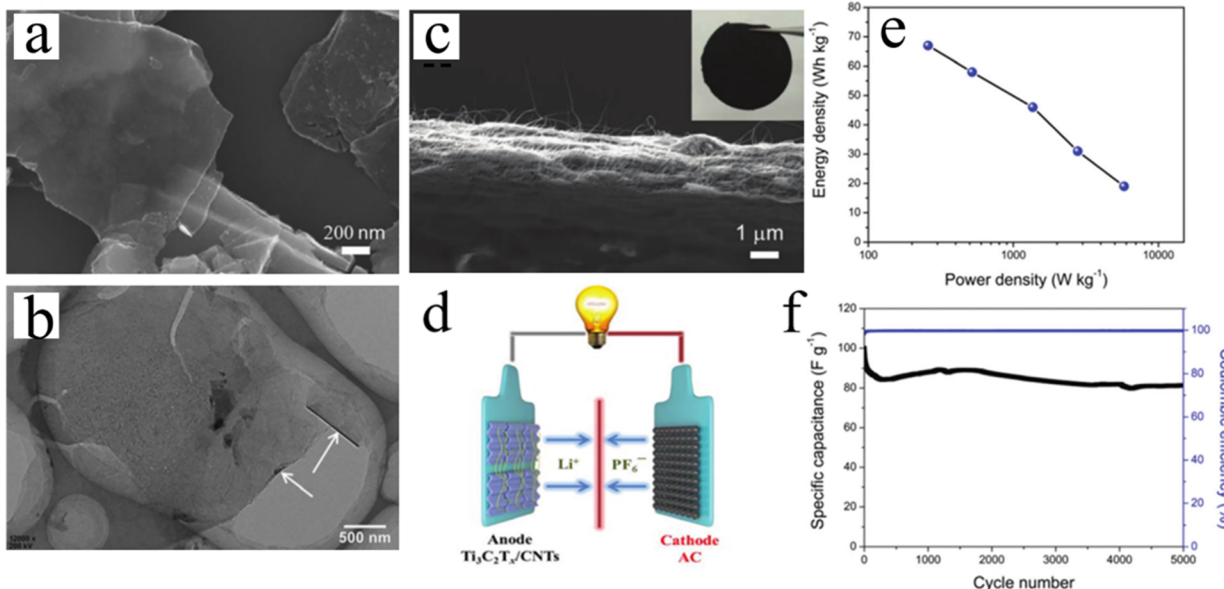


**Figure 4.** (a) SEM and (b) TEM images of delaminated Ti<sub>3</sub>C<sub>2</sub>T<sub>x</sub>. (c) SEM image of the Ti<sub>3</sub>C<sub>2</sub>T<sub>x</sub>/CNT film. (d) Schematic of the assembled Ti<sub>3</sub>C<sub>2</sub>T<sub>x</sub>/CNT//AC LIC. (e) The Ragone diagram of the LIC. (f) The cycling stability of the LIC<sup>4</sup> (reprinted with permission from ref 4).

Even though stearyltrimethylammonium bromide (STAB)@Ti<sub>3</sub>C<sub>2</sub> (50 °C–60 °C) has the largest interlayer space (2.708 nm), the high temperature causes the formation of partial TiO<sub>x</sub> on the surface of Ti<sub>3</sub>C<sub>2</sub>T<sub>x</sub> (Figure 3b). By immersing CTAB@Ti<sub>3</sub>C<sub>2</sub> in SnCl<sub>4</sub> solution, CTA<sup>+</sup> can successfully integrate Sn<sup>4+</sup> into CTAB@Ti<sub>3</sub>C<sub>2</sub> (Figure 3c,d) via an ion-exchange mechanism. The elemental mappings of Ti and Sn confirm that Sn<sup>4+</sup> is inserted in the interlayer space of CTAB@Ti<sub>3</sub>C<sub>2</sub>

(Figure 3e,f). Furthermore, an LIC is assembled with CTAB-Sn(IV)@Ti<sub>3</sub>C<sub>2</sub> as the anode and AC as the cathode (Figure 3g). The CV curves of LIC are presented in Figure 3h. The deviation from the expected rectangular shape is caused by the different energy-storage mechanisms between the anode and cathode, but the shape can still maintain unchanged as the scan rates increase from 2 to 20 mV s<sup>-1</sup>. The GCD profiles of CTAB@Ti<sub>3</sub>C<sub>2</sub>//AC LIC exhibit a symmetry triangular shape

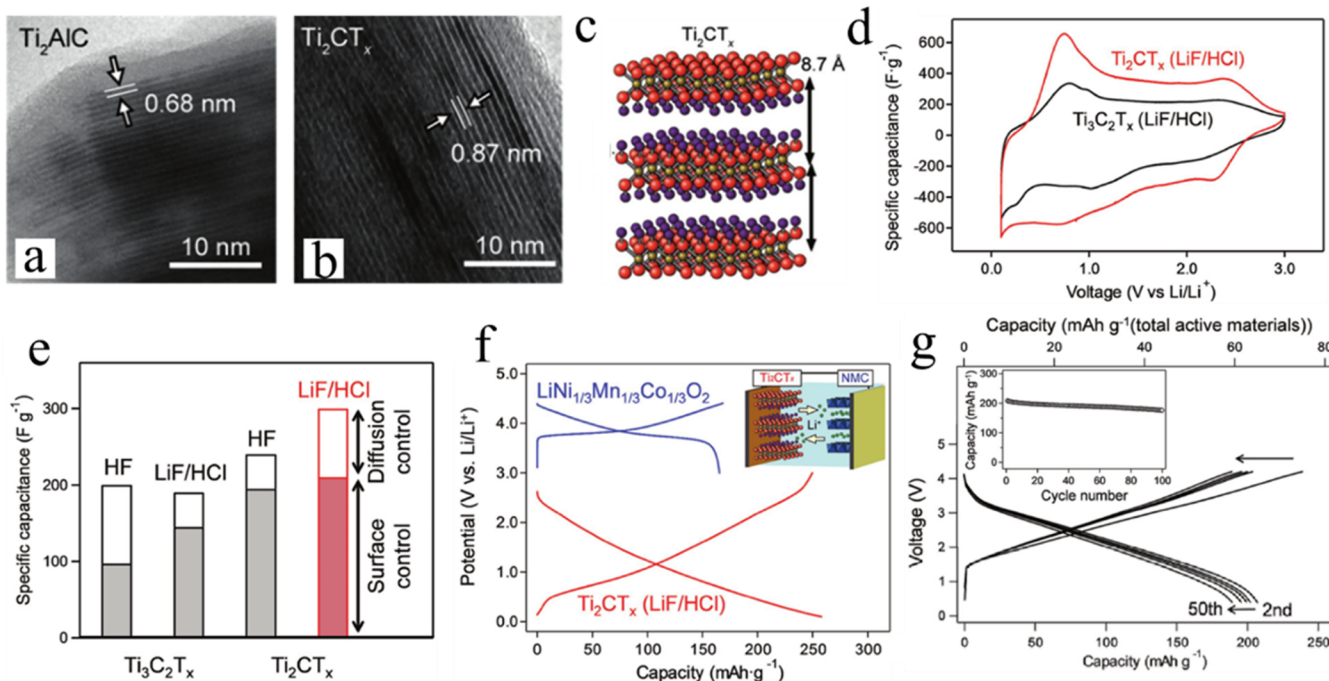


**Figure 5.** (a, b) TEM images of  $\text{Ti}_2\text{AlC}$  and  $\text{Ti}_2\text{CT}_x$  (LiF/HCl). (c) Schematic illustration of the  $\text{Ti}_2\text{CT}_x$  (LiF/HCl). (d) Cyclic voltammetry for  $\text{Ti}_2\text{CT}_x$  (LiF/HCl) and  $\text{Ti}_3\text{C}_2\text{T}_x$  (LiF/HCl) at a sweep rate of  $0.1 \text{ mV s}^{-1}$ . (e) Rate-dependent diffusion-control and rate-independent surface-control capacitances for  $\text{Ti}_3\text{C}_2\text{T}_x$  (HF),  $\text{Ti}_3\text{C}_2\text{T}_x$  (LiF/HCl),  $\text{Ti}_2\text{CT}_x$  (HF), and  $\text{Ti}_2\text{CT}_x$  (LiF/HCl) at a sweep rate of  $2 \text{ mV s}^{-1}$ . (f) Schematic illustration for LIC and charge–discharge curves of  $\text{Ti}_2\text{CT}_x$  (LiF/HCl) and  $\text{LiNi}_{1/3}\text{Mn}_{1/3}\text{Co}_{1/3}\text{O}_2$  versus  $\text{Li}/\text{Li}^+$ . (g) Charge/discharge curves and cycle performance of LIC at  $300 \text{ mA g}^{-1}$  (total active materials) (reprinted with permission from ref 21).

in Figure 3i. Based on the total active substance mass of the anode and cathode, the LIC device can reach an excellent capacitance of  $51 \text{ F g}^{-1}$ , and the LIC confirms a high energy density of  $105.56 \text{ Wh kg}^{-1}$  at the power density of  $495 \text{ W kg}^{-1}$ . Meanwhile, as shown in Figure 3j, the LIC can maintain 71.1% of initial capacity at the current density of  $2 \text{ A g}^{-1}$  after 4000 cycles.

Previous studies have revealed that the delaminated MXenes can store more charge than their multilayer counterparts.<sup>24</sup> The facile functional groups ( $T$ ) on the surface of  $\text{Ti}_3\text{C}_2\text{T}_x$  determine that the binding forces of the interlayer are weak hydrogen bonding and van der Waals' force. It provides a higher possibility to acquire delaminated  $\text{Ti}_3\text{C}_2\text{T}_x$  through intercalating dimethyl sulfoxide (DMSO), tetrabutylammonium hydroxide (TBAOH), or cation into the interlayer space.<sup>25</sup> Meanwhile, MXenes have good mechanical property that allow them to be shaped into thin films by rolling or vacuum filtration.<sup>9</sup> The freestanding MXene films can be directly employed as the electrodes without other current collectors such as Cu and Al metals. This unique flexibility is very beneficial for reducing the overall mass of the device and preparing the flexible LICs. Yu et al. mixed a delaminated  $\text{Ti}_3\text{C}_2\text{T}_x$  with carbon nanotubes to fabricate a self-supporting film anode ( $\text{Ti}_3\text{C}_2\text{T}_x/\text{CNT}$ ) for LIC. In order to obtain delaminated  $\text{Ti}_3\text{C}_2\text{T}_x$ , the cationic reagent TBA<sup>+</sup> is used as intercalation, and then ultrasonic treatment is employed.<sup>4</sup> As shown in Figure 4a,  $\text{Ti}_3\text{C}_2\text{T}_x$  is delaminated into a few or single layer, and the edge of delaminated  $\text{Ti}_3\text{C}_2\text{T}_x$  is discovered to be curved (Figure 4b), which demonstrates that its flexibility is identical to that of graphene. Moreover, the delaminated  $\text{Ti}_3\text{C}_2\text{T}_x$  nanosheets and CNTs under the vacuum filtration conditions can prepare a free-standing electrode (Figure 4c). As a pillar, the CNT looks like fishing nets wrapping the

delaminated  $\text{Ti}_3\text{C}_2\text{T}_x$ , which can prevent the restacking of  $\text{Ti}_3\text{C}_2\text{T}_x$  and increase its conductivity. The LIC, which is assembled by  $\text{Ti}_3\text{C}_2\text{T}_x/\text{CNT}$  as an anode and AC as a cathode, confirms an energy density of  $67 \text{ Wh kg}^{-1}$  (based on the total mass of  $\text{Ti}_3\text{C}_2\text{T}_x/\text{CNTs}$  and AC). Even at a power density of  $5.79 \text{ kW kg}^{-1}$ , the energy density can still reach  $19 \text{ Wh kg}^{-1}$ . Furthermore, after 5000 cycles at  $2 \text{ A g}^{-1}$ , the capacity retention of LIC is 81.3%, and the Coulombic efficiency is nearly 100% during the cycling test (Figure 4f).

**2.2.  $\text{M}_2\text{XT}_x$  MXenes.** The structure of MXenes can be represented via the general formula  $\text{M}_{n+1}\text{X}_n\text{T}_x$ .<sup>22</sup> Compared to the  $\text{M}_3$  ("M" chemistry) and  $\text{M}_4$  structures, their  $\text{M}_2$  counterparts show higher Li-ion specific capacities because  $\text{M}_2$  has less layers (2 layers) compared with previous 5 and 7 atomic layers.<sup>24</sup> Yamada et al. assembled a LIC device, which is comprised of the intercalation-type ( $\text{LiNi}_{1/3}\text{Co}_{1/3}\text{Mn}_{1/3}\text{O}_2$ ) electrode and pseudocapacitive electrode ( $\text{Ti}_2\text{CT}_x$ ).<sup>21</sup> The relationship between various surface termination groups ( $T$ ) on  $\text{Ti}_2\text{CT}_x$  and the interlayer distance ( $d_{\text{inter}}$ ) is also analyzed. As shown in Figure 5a–c, different from etching in HF (7.7 Å), the  $\text{Ti}_2\text{CT}_x$  synthesized by LiF/HCl carries a longer  $d_{\text{inter}}$  (8.7 Å). The reason is the presence of the new component of the termination group ( $T = -\text{Cl}$ ), and the  $d_{\text{inter}}$  for surface termination ( $T$ ) combinations presents a continuous increase with the addition of  $-\text{Cl}$ . The enlargement of interlayer spacing offers a fast ionic accessibility to redox centers, thus exhibiting higher intercalation pseudocapacitance. As demonstrated in Figure 5d, 250  $\text{mAh g}^{-1}$  capacity of the  $\text{Ti}_2\text{CT}_x$  is much larger than that of LiF/HCl etching of  $\text{Ti}_3\text{C}_2\text{T}_x$  (150  $\text{mAh g}^{-1}$ ). In addition, the permeation of solvent molecules will further increase the interlayer space during the charging–discharging process. The rate performance of LICs is usually limited by the diffusion capacity of lithium ions. In this system,

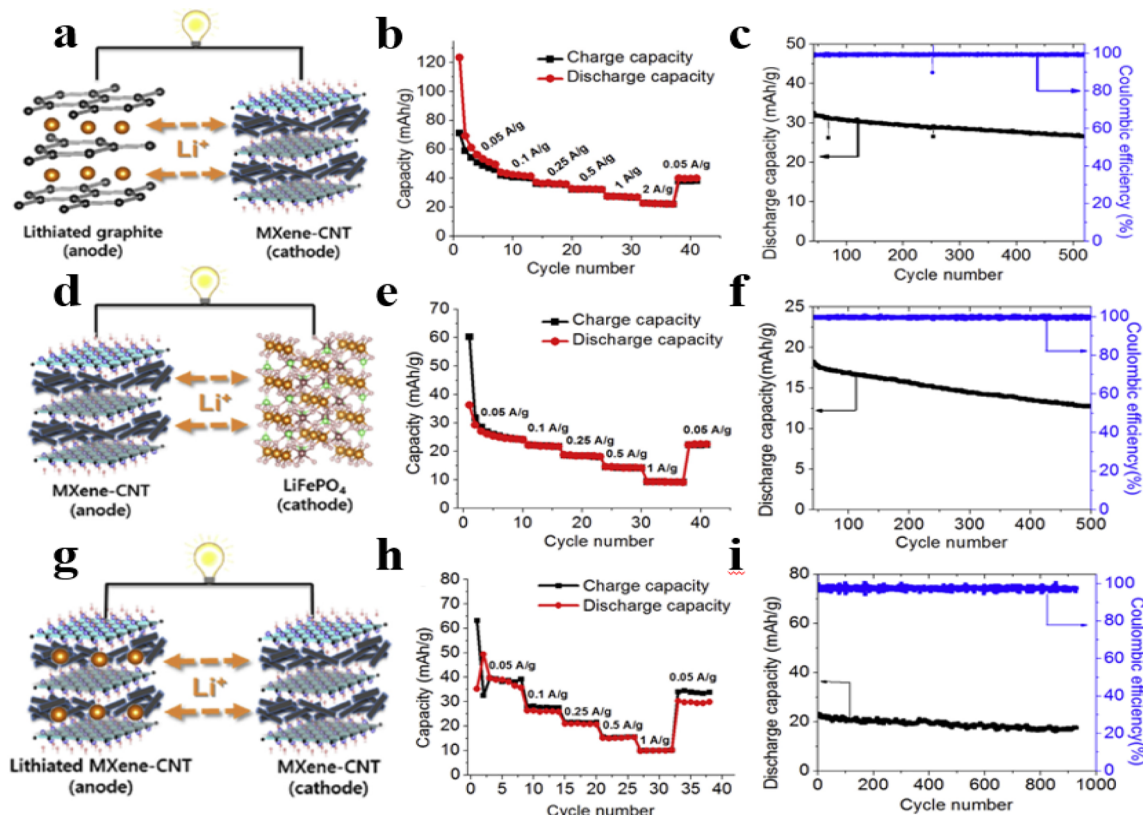


**Figure 6.** (a–c) Lithiated graphite/Nb<sub>2</sub>CT<sub>x</sub>-CNT capacitor, rate capability test, and the subsequent cyclic stability test at a current rate of 250 mA/(g of Nb<sub>2</sub>CT<sub>x</sub>-CNT). (d–f) Nb<sub>2</sub>CT<sub>x</sub>-CNT/LiFePO<sub>4</sub> capacitor, rate capability test, and the subsequent cyclic stability test at a current rate of 250 mA/(g of Nb<sub>2</sub>CT<sub>x</sub>-CNT). (g–i) Lithiated Nb<sub>2</sub>CT<sub>x</sub>-CNT/Nb<sub>2</sub>CT<sub>x</sub>-CNT capacitor, rate capability test, and the subsequent cyclic stability test at a current rate of 250 mA/(g of Nb<sub>2</sub>CT<sub>x</sub>-CNT)<sup>19</sup> (reprinted with permission from ref 19).

the interlayer space is expanded with the embedding of  $\text{Cl}^-$ , and the large interlayer space boosts the faster Li-ion diffusion. Thus, at a sweep rate less than  $2 \text{ mV s}^{-1}$ , the capacitance of diffusion control in Ti<sub>2</sub>CT<sub>x</sub> (LiF/HCl) is the largest among various Ti<sub>n+1</sub>C<sub>n</sub>T<sub>x</sub> (Figure 5e). Therefore, Ti<sub>2</sub>CT<sub>x</sub> (LiF/HCl) as the capacitor-type anode for LIC can provide a higher rate capability. A Li-ion hybrid capacitor is assembled as shown in Figure 5f, exhibiting a high capacity of  $206 \text{ mAh g}^{-1}$  in a voltage window of  $2.58 \text{ V}$ , and  $84\%$  of capacity is maintained after the 100 cycles (Figure 5g). Meanwhile, the LIC displays an energy density ( $160 \text{ Wh kg}^{-1}$ ) at a power density ( $220 \text{ W kg}^{-1}$ ) based on the total active materials.

According to the experimental data of the lithium half battery, the specific capacities of Ti<sub>3</sub>C<sub>2</sub>T<sub>x</sub> and Ti<sub>2</sub>CT<sub>x</sub> are less than that of Nb<sub>2</sub>CT<sub>x</sub> and V<sub>2</sub>CT<sub>x</sub>. The delaminating process of Nb<sub>2</sub>CT<sub>x</sub> often uses different chemical approaches than that of Ti<sub>3</sub>C<sub>2</sub>T<sub>x</sub>. Olha et al. reported the delamination of Nb<sub>2</sub>CT<sub>x</sub> using amine instead of DMSO. Then, the Nb<sub>2</sub>CT<sub>x</sub> paper was obtained by mixing the delaminated Nb<sub>2</sub>CT<sub>x</sub> suspension with CNTs and filtering through a polyester membrane. The Nb<sub>2</sub>CT<sub>x</sub>/CNT paper electrode shows a high volumetric capacitance of  $325 \text{ F cm}^{-3}$ .<sup>24</sup> Ayeong et al. demonstrated three proof-of-concept type LICs based on TBAOH-delaminated Nb<sub>2</sub>CT<sub>x</sub>/CNT electrodes. The Nb<sub>2</sub>CT<sub>x</sub>/CNT can be paired with either a graphite anode or a LiFePO<sub>4</sub> cathode. Furthermore, a symmetric capacitor is assembled using the Nb<sub>2</sub>CT<sub>x</sub>/CNT electrodes as the anode and cathode (Figure 6a–i).<sup>19</sup> Three type of LIC devices are capable of operating within a  $3 \text{ V}$  voltage window and delivering stabilized capacities of  $43$ ,  $24$ , and  $36 \text{ mA g}^{-1}$ , respectively. Continuous

cycling of LICs demonstrated long lifespan for all three types of LICs, and the volumetric energy densities of all LICs are  $50$ – $70 \text{ Wh L}^{-1}$  (based on the volume of electrodes), which exceed the energy density of the conventional LTO/AC LIC.

In general, all kinds of MXenes display a layered structure, and the skeleton atoms of MXenes follow the ABABA or ABCABC arrangement. Meanwhile, the terminated groups ( $-\text{F}$ ,  $-\text{OH}$ ,  $-\text{O}$ , et al.) on the surface of MXenes directly influence their chemical/physical properties and then determine the performance of MXenes in their applications. In the field of energy storage, MXenes are often used as a substrate and further improve the performance through a series of chemical modifications. Through analyzing the electrochemical data of LICs assembled using MXenes or MXene composites, the capacitance is mainly a diffusion-controlled contribution, and it is worth noting that the surface control contribution cannot be ignored. Therefore, MXene materials have shown great potential in the lithium-ion capacitors.

### 3. CONCLUSIONS AND OUTLOOK

In summary, searching the novel electrode materials for a lithium-ion capacitor plays a really important role in development of electrochemical energy storage. MXenes, as the new star in the family of 2D materials, have attracted increasing attention because of their metallic skeleton, structural varieties, and substantial surface termination groups. The 2D nature of MXenes provides large surface areas for lithium-ion storage and boosts the fast ion transport. It is observed that MXenes exhibit some potential as a substrate material for the lithium-

**Table 1.** Comparison of MXenes and MXene-Based Materials for LIC Applications

materials	synthesis approach	capacity of anode	working voltage for LIC	electrochemical performance for LIC	cycle number and capacitance retention for LIC	ref
Ti <sub>3</sub> C <sub>2</sub> T <sub>x</sub> @Fe <sub>2</sub> O <sub>3</sub>	surfactant	1180 mAh g <sup>-1</sup> at 0.1 A g <sup>-1</sup>	0.01–4 V 1 M LiPF <sub>6</sub> nonaqueous solution	216 Wh kg <sup>-1</sup> at 400 W kg <sup>-1</sup>	5000 (87%)	23
CTAB-Sn(IV)@Ti <sub>3</sub> C <sub>2</sub>	liquid-phase immersion	765 mAh g <sup>-1</sup> at 0.1 A g <sup>-1</sup>	1–4 V 1 M LiPF <sub>6</sub> nonaqueous solution	105.6 Wh kg <sup>-1</sup> at 495 W kg <sup>-1</sup>	4000 (71.1%)	5
delaminated Ti <sub>3</sub> C <sub>2</sub> T <sub>x</sub> /CNT	TBAOH delamination and filtration	489 mAh g <sup>-1</sup> at 50 mA g <sup>-1</sup>	1–4 V 1 M LiPF <sub>6</sub> nonaqueous solution	67 Wh kg <sup>-1</sup> at 258 W kg <sup>-1</sup>	5000 (81.3%)	4
Ti <sub>2</sub> CT <sub>x</sub>	etching by LiF/HCl	250 mAh g <sup>-1</sup> at 20 mA g <sup>-1</sup>	0.4–4.2 V 1 M LiPF <sub>6</sub> nonaqueous solution	160 Wh kg <sup>-1</sup> at 220 W kg <sup>-1</sup>	100 (84%)	21
Nb <sub>2</sub> CT <sub>x</sub> /CNT paper	amine-assisted delamination and filtration	400 mAh g <sup>-1</sup> at 0.5 C	—	325 F cm <sup>-3</sup>	—	24
delaminated Nb <sub>2</sub> CT <sub>x</sub> /CNT	TBAOH delamination and filtration	270 mAh g <sup>-1</sup> at 50 mA g <sup>-1</sup>	0–3 V 1 M LiPF <sub>6</sub> nonaqueous solution	50–70 Wh L <sup>-1</sup>	—	19
Ti <sub>3</sub> C <sub>2</sub> T <sub>x</sub>	etching by LiF/HCl	226 F cm <sup>-3</sup> at 10 mV s <sup>-1</sup>	0–2 V 1 M Li <sub>2</sub> SO <sub>4</sub> aqueous solution	20.7 μWh cm <sup>-2</sup> at 2.2 mW cm <sup>-2</sup>	—	20

ion capacitor. Meanwhile, it has been proven that the surface terminations such as  $-\text{OH}$ ,  $-\text{O}$ ,  $-\text{F}$ , or  $-\text{Cl}$  greatly affect the structural characteristic and electrochemical performance of MXenes. These functional groups and the binding force of the MXene interlayer are weak hydrogen bonding and van der Waals' force, and these functional groups maintain a stable space in between the MXene layers. The advantages of 2D MXenes for the lithium-ion capacitor have been confirmed theoretically and experimentally. This mini-review is mainly focused on the structural design and performance optimization of MXenes by cation intercalation, delamination, and compositing with other materials. Various lithium-ion capacitor systems assembled by MXenes or MXene composites are summarized and discussed in detail. The main electrochemical properties of these LICs are listed in Table 1. Although this paper is focused on the research of MXenes for LICs, the preparation routes and structure designs of MXenes and MXene-based materials, which possess ideal 2D structure, large interlayer space, and metal conductivity, are also valuable for studying  $\text{Na}^+$ ,  $\text{K}^+$ ,  $\text{Mg}^{2+}$ , and other metal-ion hybrid capacitors.

Recently, the main disadvantage of the lithium-ion capacitors is their low energy density (compared to batteries), and the unmodified MXene electrodes do not have considerable theoretical capacity. Thus, anchoring the active substance on the nanosheets or delaminating the multilayer to monolayer are the practical methods to improve the electrochemical performance of MXenes. Although abundant examples of 2D MXenes in energy-storage applications have been performed, there are still some underlying scientific issues for the structure-electrochemical property to be addressed. First, the indispensability of the fluoride based (HF and LiF) on the process of etchants increases the risk. Searching for safe and reliable preparation methods is beneficial to the future development of MXenes. Second, single-layer MXenes are fabricated by delaminating multilayered MXenes in order to expose more lithium-ion storage active sites, but the delaminated MXenes in aqueous solution show a trend of restacking due to electrostatic interaction. Although the introduction of other substances as pillars can expand the interlayer space of MXenes, these also reduce the contact area between MXenes and electrolyte that impede their intrinsic properties in some cases. Third, since MXenes are unstable under ambient conditions, most MXenes are easily oxidized and degraded during treatment. The exploitation of the

MXene-based hybrid system, such as anchoring self-assembly, delamination, insertion, and anchoring, is impossible to completely isolate oxygen and water. Therefore, the chemical stability control of MXenes still needs further investigation. Fourth, because the surface termination groups of MXenes are diverse and uncontrollable, the ion kinetics and charge storage mechanism for MXenes remain not completely clear. Compared to the lithium-ion battery, the main advantage of LICs is its high power density, and the ion transport speed of the battery-type electrode directly determines the rate performance of the device. Thus, in-depth basic studies of the lithium-ion storage mechanism for MXenes are needed tremendously.

Many breakthroughs of MXene and MXene composites, which are used as lithium-ion capacitor electrodes, have emerged in the past few years. However, there is indeed a long way to go to find solutions that balance various performances such as energy density and power density, specific capacity, and life span. In order to address the challenges, innovative works and practical applications of electrochemical energy storage are still desirable to further explore.

## ■ AUTHOR INFORMATION

### Corresponding Author

\*E-mail: [ywma@mail.iee.ac.cn](mailto:ywma@mail.iee.ac.cn) (Y. Ma).

### ORCID

Xiong Zhang: 0000-0001-9760-5206

Chen Li: 0000-0002-0947-585X

Kai Wang: 0000-0001-8836-1553

Yanwei Ma: 0000-0002-7131-0888

### Notes

The authors declare no competing financial interest.

## ■ ACKNOWLEDGMENTS

This work was financially supported by the National Natural Science Foundation of China (No. 51677182 and 51822706), the DNL Cooperation Fund (DNL201915), the Beijing Municipal Science and Technology Commission (No. Z181100000118006), and the Beijing Nova Program (No. Z171100001117073).

## ■ REFERENCES

- (1) She, L.; Yan, Z.; Kang, L.; He, X.; Lei, Z.; Shi, F.; Xu, H.; Sun, J.; Liu, Z. H. Nb<sub>2</sub>O<sub>5</sub> Nanoparticles Anchored on an N-Doped Graphene

- Hybrid Anode for a Sodium-Ion Capacitor with High Energy Density. *ACS Omega* **2018**, *3*, 15943–15951.
- (2) Sun, Y.; Liu, N.; Cui, Y. Promises and challenges of nanomaterials for lithium-based rechargeable batteries. *Nat. Energy* **2016**, *1*, 16071.
- (3) Zhang, J. M.; Hua, Q.; Li, J.; Yuan, J.; Peijs, T.; Dai, Z.; Zhang, Y.; Zheng, Z.; Zheng, L.; Tang, J. Cellulose-Derived Highly Porous Three-Dimensional Activated Carbons for Supercapacitors. *ACS Omega* **2018**, *3*, 14933–14941.
- (4) Yu, P.; Cao, G.; Yi, S.; Zhang, X.; Li, C.; Sun, X.; Wang, K.; Ma, Y. Binder-free 2D titanium carbide (MXene)/carbon nanotube composites for high-performance lithium-ion capacitors. *Nanoscale* **2018**, *10*, 5906–5913.
- (5) Luo, J.; Zhang, W.; Yuan, H.; Jin, C.; Zhang, L.; Huang, H.; Liang, C.; Xia, Y.; Zhang, J.; Gan, Y.; Tao, X. Pillared Structure Design of MXene with Ultralarge Interlayer Spacing for High-Performance Lithium-Ion Capacitors. *ACS Nano* **2017**, *11*, 2459–2469.
- (6) Jiang, H.; Lee, P. S.; Li, C. 3D carbon based nanostructures for advanced supercapacitors. *Energy Environ. Sci.* **2013**, *6*, 41–53.
- (7) Dubal, D. P.; Jayaramulu, K.; Sunil, J.; Kment, S.; Gomez-Romero, P.; Narayana, C.; Zboril, R.; Fischer, R. A. Metal-Organic Framework (MOF) Derived Electrodes with Robust and Fast Lithium Storage for Li-Ion Hybrid Capacitors. *Adv. Funct. Mater.* **2019**, *29*, 1900532.
- (8) Yu, H.; Wang, Y.; Jing, Y.; Ma, J.; Du, C. F.; Yan, Q. Surface Modified MXene-Based Nanocomposites for Electrochemical Energy Conversion and Storage. *Small* **2019**, *15*, 1901503.
- (9) Xiong, D.; Li, X.; Bai, Z.; Lu, S. Recent Advances in Layered  $Ti_3C_2T_x$  MXene for Electrochemical Energy Storage. *Small* **2018**, *14*, 1703419.
- (10) Li, B.; Zheng, J.; Zhang, H.; Jin, L.; Yang, D.; Lv, H.; Shen, C.; Shellikeri, A.; Zheng, Y.; Gong, R.; Zheng, J. P.; Zhang, C. Electrode Materials, Electrolytes, and Challenges in Nonaqueous Lithium-Ion Capacitors. *Adv. Mater.* **2018**, *30*, 1705670.
- (11) Aravindan, V.; Jayaraman, S.; Tedjar, F.; Madhavi, S. From Electrodes to Electrodes: Building High-Performance Li-Ion Capacitors and Batteries from Spent Lithium-Ion Battery Carbonaceous Materials. *ChemElectroChem* **2019**, *6*, 1407–1412.
- (12) Bonaccorso, F.; Colombo, L.; Yu, G.; Stoller, M.; Tozzini, V.; Ferrari, A. C.; Ruoff, R. S.; Pellegrini, V. 2D materials. Graphene, related two-dimensional crystals, and hybrid systems for energy conversion and storage. *Science* **2015**, *347*, 1246501.
- (13) Chen, Z.; Ren, W.; Gao, L.; Liu, B.; Pei, S.; Cheng, H. M. Three-dimensional flexible and conductive interconnected graphene networks grown by chemical vapour deposition. *Nat. Mater.* **2011**, *10*, 424–428.
- (14) Anasori, B.; Lukatskaya, M. R.; Gogotsi, Y. 2D metal carbides and nitrides (MXenes) for energy storage. *Nat. Rev. Mater.* **2017**, *2*, 16098.
- (15) Zhang, C. J.; Anasori, B.; Seral-Ascaso, A.; Park, S. H.; McEvoy, N.; Shmeliiov, A.; Duesberg, G. S.; Coleman, J. N.; Gogotsi, Y.; Nicolosi, V. Transparent, Flexible, and Conductive 2D Titanium Carbide (MXene) Films with High Volumetric Capacitance. *Adv. Mater.* **2017**, *29*, 1702678.
- (16) Yang, W.; Yang, J.; Byun, J. J.; Moissinac, F. P.; Xu, J.; Haigh, S. J.; Domingos, M.; Bissett, M. A.; Dryfe, R. A. W.; Barg, S. 3D Printing of Freestanding MXene Architectures for Current-Collector-Free Supercapacitors. *Adv. Mater.* **2019**, *31*, 1902725.
- (17) Yang, J.; Bao, W.; Jaumaux, P.; Zhang, S.; Wang, C.; Wang, G. MXene-Based Composites: Synthesis and Applications in Rechargeable Batteries and Supercapacitors. *Adv. Mater. Interfaces* **2019**, *6*, 1802004.
- (18) Nan, J.; Guo, X.; Xiao, J.; Li, X.; Chen, W.; Wu, W.; Liu, H.; Wang, Y.; Wu, M.; Wang, G. Nanoengineering of 2D MXene-Based Materials for Energy Storage Applications. *Small* **2019**, 1902085.
- (19) Byeon, A.; Glushenkov, A. M.; Anasori, B.; Urbankowski, P.; Li, J.; Byles, B. W.; Blake, B.; Van Aken, K. L.; Kota, S.; Pomerantseva, E.; Lee, J. W.; Chen, Y.; Gogotsi, Y. Lithium-ion capacitors with 2D  $Nb_2CT_x$  (MXene)-carbon nanotube electrodes. *J. Power Sources* **2016**, *326*, 686–694.
- (20) Li, J.; Kurra, N.; Seredych, M.; Meng, X.; Wang, H.; Gogotsi, Y. Bipolar carbide-carbon high voltage aqueous lithium-ion capacitors. *Nano Energy* **2019**, *56*, 151–159.
- (21) Kajiyama, S.; Szabova, L.; Inuma, H.; Sugahara, A.; Gotoh, K.; Sodeyama, K.; Tateyama, Y.; Okubo, M.; Yamada, A. Enhanced Li-Ion Accessibility in MXene Titanium Carbide by Steric Chloride Termination. *Adv. Energy Mater.* **2017**, *7*, 1601873.
- (22) Jun, B. M.; Kim, S.; Heo, J.; Park, C. M.; Her, N.; Jang, M.; Huang, Y.; Han, J.; Yoon, Y. Review of MXenes as new nanomaterials for energy storage/delivery and selected environmental applications. *Nano Res.* **2019**, *12*, 471–487.
- (23) Tang, X.; Liu, H.; Guo, X.; Wang, S.; Wu, W.; Mondal, A. K.; Wang, C.; Wang, G. A novel lithium-ion hybrid capacitor based on an aerogel-like MXene wrapped  $Fe_2O_3$  nanosphere anode and a 3D nitrogen sulphur dual-doped porous carbon cathode. *Mater. Chem. Front.* **2018**, *2*, 1811–1821.
- (24) Mashtalir, O.; Lukatskaya, M. R.; Zhao, M. Q.; Barsoum, M. W.; Gogotsi, Y. Amine-Assisted Delamination of  $Nb_2C$  MXene for Li-Ion Energy Storage Devices. *Adv. Mater.* **2015**, *27*, 3501–3506.
- (25) Tang, H.; Hu, Q.; Zheng, M.; Chi, Y.; Qin, X.; Pang, H.; Xu, Q. MXene-2D layered electrode materials for energy storage. *Prog. Nat. Sci.* **2018**, *28*, 133–147.